Histol Histopathol (2018) 33: 1099-1110

http://www.hh.um.es

Histology and Histopathology

From Cell Biology to Tissue Engineering

Quantification of the heterogeneity of cytokeratin 18 immunoexpression in prostate adenocarcinoma and normal prostate: Global and local features

Luis Santamaría[1], Ildefonso Ingelmo[2], Bryan Sinues[3], Laura Martínez[3] and Fernando Teba[4]

[1]Department of Anatomy, Histology, and Neuroscience, School of Medicine, Autonomous University of Madrid, [2]Department of Anesthesiology, Hospital Ramón y Cajal, [3]Service of Urology, Hospital del Henares and [4]Department of Surgery (Urology), Hospital de La Princesa, School of Medicine, Autonomous University of Madrid, Madrid, Spain

Summary. There are few studies comparing global versus local changes in spatial patterns in prostate cancer. In this study, stereological tools have been applied to find out if the cytokeratin18 (ck18) immunoexpression shows local changes in cancer compared to normal prostate. To verify if these changes are relevant to ascertain differences between normal (CTR) and cancer (Ca) cases, several parameters were estimated. Volume fraction of epithelium immunostained for ck18 (V_V ck18), dispersion index of V_V ck18, positional variance of V_V ck18, and multiscale entropy analysis (MSE) to measure the tissue heterogeneity. The MSE values showing significant differences between CTR and Ca were employed in a discriminant analysis to determine if MSE was able to classify the cases in CTR and Ca groups. The findings obtained indicate that changes in the expression of ck18 by the cancer prostate are heterogeneous. The increase in local variability of ck18 immunoexpression can be related to the increase in heterogeneity of shape and size of the tumor acini. The asymmetry of distribution of the local values of V_V ck18 along the axis of the space series may indicate the existence of anisotropy in the distribution of tumor acini. The increase in scale-dependent entropy for V_V ck18 in cancer at the morphological level could be interpreted as the macroscopic expression of the same increase at the molecular level already described. The discriminant analysis shows that the dependence on the resolution for MSE values need to be taken into account to characterize the prostate cancer better.

Key words: Cancer prostate, Cytokeratin 18, Local changes, Multiscale entropy

Offprint requests to: Luis Santamaría, Department of Anatomy, Histology and Neuroscience, School of Medicine, UAM, C/ Arzobispo Morcillo, 2; 28029-Madrid, Spain. e-mail: luis.santamaria@uam.es

DOI: 10.14670/HH-18-009

Introduction

Prostate cancer is a complex system consisting of different cell clones that interact with each other and also with normal cells, these sort of interactions are the frequent cause of intratumor heterogeneity that is observed at different stages of tumor progression, metastasis, and recurrence (Park et al., 2016). Although prostate carcinoma remains one of the most common carcinomas affecting the male population, little is known about the variability of local changes in the expression of different markers and their relationship with the behavior of the tumor.

The cytokeratin class of intermediate filaments has been shown to exist in all epithelia (Franke et al., 1979). There are now recognized 19 distinct cytokeratins expressed in human epithelia, and each epithelial type has a different phenotype concerning these proteins (Moll et al., 1982; Quinlan et al., 1985). Early studies using polyclonal anti-cytokeratins demonstrated that the basal cells of the prostate have cytokeratins that were showing different immunoreactivities from the luminal or columnar cells (Schlegel et al., 1980; Barwick and Mardi, 1983). Several studies using monoclonal anti-

cytokeratin antibodies have differentiated the columnar and basal cell populations by their specific cytokeratin content (Brawer et al., 1985). The columnar cells react with monoclonal antibodies to cytokeratin 18 (ck18) (Nagle et al., 1987). Besides, chemical determination of the cytokeratin phenotype of three established human prostatic carcinoma cell lines also suggests that all three cell lines synthesize ck18 (Nagle et al., 1987). When comparing the immunoexpression of ck18 in benign prostate hyperplasia (BPH) with normal prostate, no remarkable differences are detected (Nagle et al., 1987; Verhagen et al., 1992). Nevertheless, the percentage of positivity for luminal ck18 was statistically lower for BPH cultures with respect to the positivity observed for both prostatic intraepithelial neoplasia (PIN) and prostate cancer-derived cultures (Festuccia et al., 2005).

The comparison between global versus local changes in spatial patterns of pathological lesions has provoked a growing interest in some fields such as neuropathology (Armstrong et al., 2001). However, there is little data on this subject in the field of prostatic pathology. Recently, several studies have dealt with the estimation of measurements of either acinar or stromal parameters at the local level in normal and pathological prostate, using second-order stereological methods (Howard and Reed, 2005). These studies make reference to the patterning of prostate, distribution and isotropy of nuclei population and prostate acini, etc.(Santamaria et al., 2011, 2015, 2016, 2017; Santamaría Solis et al., 2015). In some of these studies, several discrepancies between global and local results were detected. Thus, the first order (global) parameter of the volume fraction of epithelial ck18 does not show differential information between normal and cancer prostate acini (Santamaría Solis et al., 2015). Moreover, in the study of the structural pattern of the acinar tree, the global measurements such as the average volume of acini were unable to distinguish between normal prostate and BPH, whereas local parameters, such as connectivity density, showed remarkable differences between normal and hyperplastic prostate (Santamaria et al., 2016). On the other hand in the prostatic hyperplasia, the local changes in ck18 were more evident regarding volume fraction of ck18 immunoexpression and its local variability, whereas other parameters that are useful in other pathologies, such as lacunarity, are less relevant (Santamaria et al., 2017).

One of the essential characteristics of cancer cells is an increased phenotypic plasticity, driven by underlying genetic and epigenetic perturbations. However, at a systems-level, it is unclear how these perturbations give rise to the observed increased plasticity. Recently, it has been shown that signaling entropy, an overall measurement of signaling pathway mesh, correlates with phenotypic plasticity and is increased in cancer compared to normal tissue (Teschendorff et al., 2015). Then, it seems interesting to apply a multiscale entropy analysis (MSE) (Costa et al., 2000, 2002, 2005; Gao et al., 2015) in order to ascertain if there are local variations of ck18 immunoexpression in prostate cancer accounting for a change in the tissue complexity in comparison with normal prostate.

Traditional methods quantify the degree of regularity of a space series by evaluating the appearance of repetitive patterns. However, there is no straightforward correspondence between regularity, which can be measured by entropy-based algorithms, and complexity. Intuitively, complexity is associated with "meaningful structural richness" which, in contrast to the outputs of random phenomena, exhibits relatively higher regularity. Entropy-based measurements, such as the entropy rate and the Kolmogorov complexity, grow monotonically with the degree of randomness. Therefore, these measures assign the highest values to uncorrelated random signals such as white noise, which is highly unpredictable but not structurally complex, and, at a global level, admit a straightforward description. In the present study, the MSE method developed by Costa et al. (2002, 2003, 2005), was applied to the analysis of volume fraction of immunoreactivity to ck18 in order to ascertain whether there are changes in multiscale entropy from these signals in cancer prostate compared to normal prostate.

Due to the relevance of local parameters to distinguish between normal and pathological structures, this work will apply first and second order quantitative tools to find out if the ck18 immunoexpression shows significant local changes in prostate cancer compared to normal prostate, independently if global estimates were similar in both groups.

The following parameters were applied to check for such local changes in the ck18 immunoreactivity in both normal and cancer prostate:

1- Volume fraction of epithelium immunostained for ck18 (V_V ck18), both in global and local estimates (pixel to pixel tissue).

2- Dispersion indices of global V_V ck18, such as Morisita index (Morisita 1959; Rosenberg et al., 2011).

3- Estimates of the local positional variance of V_V ck18 using wavelet analysis (Bradshaw and Spies, 1992; Bradshaw and McIntosh, 1994; Dale and Mah, 1998; Nakken 1999).

4- Multiscale entropy analysis to visualize changes in the signal complexity caused by the immunoexpression of ck18 in prostate cancer compared to the normal prostate (Costa et al., 2005).

Material and methods

Material

Twenty-five prostate specimens were collected from La Princesa Hospital (Madrid, Spain), ten were from adults, (CTR group), age (mean ± SD): 45±7; range: 30-47 years. All these specimens were of healthy subjects, without endocrine or reproductive pathology, deceased in traffic accidents, and eligible as donors for transplant. The age of the patients of CTR group was in the range indicated to avoid any histological changes of

subclinical BPH, relatively frequent in men older than 50 years. The other 15 were surgical specimens (radical prostatectomy) from patients diagnosed with prostate carcinoma (Ca group): age (mean ± SD): 70±10, range: 56 to 85 years. In all these cases, the diagnosis of carcinoma was previously confirmed by histopathology. The cancer cases were graded according to Gleason score (Epstein et al., 2005) and the average grading was 7 (3+4). All of these cases were without prior neoadjuvant hormonal therapy. Ethical requirements were adhered to when obtaining the prostatic tissue either at the moment of the multiorgan extraction for transplant (CTR group) or the surgery (Ca group).

Processing of the tissues

Immediately after extraction, the specimens were fixed for one week in 10% paraformaldehyde in PBS, pH 7.4. After fixation, the samples from the two groups were thoroughly sectioned into 2-mm-thick slices, performed by isotropic uniform random sampling (IUR sections) to preserve the isotropy of the tissue (Baddeley and Vedel Jensen, 2005).

All the specimens were processed for paraffin embedding. The paraffin blocks were exhaustively sectioned. A total of 30 sections (5-μm-thick) were performed on each block for immunohistochemistry.

Immunohistochemistry

At least ten randomly selected slides per specimen were immunostained for ck18 in CTR and Ca groups. Deparaffinized and rehydrated tissue sections were treated at room temperature for 30 min with hydrogen peroxide 0.3% in phosphate-buffered saline (PBS) pH 7.4, to block endogenous peroxidase. Sections were incubated with a monoclonal anti-cytokeratin 18 antibody (Abcam, Cambridge, UK) diluted at 1:250 to detect ck18 immunoreactivity. Pretreatment of sections by heat in citrate buffer pH 6.0 (using a pressure cooker) (Martin et al., 2001) was performed to enhance immunostaining.

The primary antiserum was diluted in PBS pH 7.4 containing 1% bovine serum albumin (BSA) (Sigma, St Louis, USA) plus 0.1% sodium azide (Merck, Darmstadt, Germany). The incubation with primary antiserum was overnight at 4°C. The second antibody employed was a biotin-caproyl-anti-rabbit immunoglobulin (Biomeda, Foster City, CA, USA). The second antibody was diluted at 1/400 in PBS containing 1% BSA without sodium azide and incubated for 30 min at room temperature. After that, sections were incubated with a streptavidin-biotin-peroxidase complex (Biomeda). The immunostaining reaction product was developed using 0.1 g diaminobenzidine (DAB) (Sigma) in 200 mL of PBS, plus 40 μL hydrogen peroxide. After immunoreaction, nuclear counter-staining with Harris hematoxylin was performed in some sections immunostained for ck18. No nuclear counter-staining was performed on the remaining sections that were then employed for quantitative purposes. All slides were dehydrated in ethanol and mounted in a synthetic resin (Depex, Serva, Heidelberg, Germany). The specificity of the immunohistochemical procedures was checked by incubation of sections with no immune serum instead of the primary antibody.

Data acquisition

Three strips of an average of 20 immediately adjacent quadrats (range 10-40) were explored for each immunostained section from CTR and Ca groups. The origin and sense of the axis for each strip were chosen by systematic random sampling (Gundersen and Osterby, 1981) for all the strips. The result was a series of images from the two groups, sized, on average, 512×7000 pixels. The final magnification (x100) was such that 1000 pixels represented 1280 μm. At that point, the strips were 9 mm long, on average. Therefore, the total length explored per section (ten sections) and per case (at least 10 cases) was 9×10×10=900 mm (for Ca cases, an appreciable percentage of the maximum specimen diameter) (Santamaria et al., 2011).

The images were captured using a color digital camera DP 70 (Olympus Corporation of the Americas, PA, USA) with a resolution of 12.5 megapixels, attached to an Olympus microscope fitted with a motorized stage controlled by the stereological software Cast-Grid (Stereology Software Package, Silkeborg, Denmark). This program monitors the XY displacement of the microscope stage and allows the selection of fields to be studied by systematic random sampling after the input of an appropriate sampling fraction (Santamaría et al., 2015).

The strips were then mounted from the images captured, using the public domain Java image processing program, Image J (version 1.48), developed at the US National Institutes of Health and available on the Internet at https://imagej.nih.gov/ij/index.html (Rasband and Bright, 1995). Subsequently, the resultant strips were processed using the same software. A binary image was produced where the immunostaining to ck18 was shown as black and the pore space (lumina of acini, stroma, etc.) as white (Figs. 1, 2).

Quantitative measurements

Volume fractions of immunostained epithelium

The local measurements of the fraction of the volume of tissue immunostained to ck18 (V_V ck18) were obtained. At each point of the long axis of each image strip, the fraction of pixels belonging to the immunostained epithelium expressed as a percentage over the space of reference (pore space plus immunoreactive epithelial component) was automatically recorded by the image analysis system for all the N columns orthogonal to the long axis. The resulting series

of N consecutive rational numbers per visual field served as input signals for estimating the V_V ck18 measurements (per pixel of tissue) (Santamaria et al., 2011). The results were plotted as a space series, being the position (number of pixels transformed on microns) represented in the X-axis and the V_V ck18 in the Y-axis of the plot.

The global measurement of V_V ck18 was obtained averaging the local V_V ck18 over the total number of strips for each case in both CTR and Ca groups.

Dispersion index of the global V_V ck18 measurements

This procedure takes estimates of V_V ck18 from quadrats and calculates several indices that can be used to identify the spatial patterning of the volume fraction. In the present study, the Morisita index (MI) was obtained (Morisita 1959). It is the scaled probability that two measurements chosen at random from the whole population are in the same quadrat. The higher the value, the more clumped the distribution. Randomization tests were performed to check whether the Morisita index of the observed data was the result of random clumping or followed a particular pattern (Santamaria et al., 2017). The order of the quadrats within the space series was randomized and the Morisita index obtained for the randomized data. These measurements were performed using the PASSaGE software (Rosenberg et al., 2011), which is a program suitable for pattern analysis and spatial statistics.

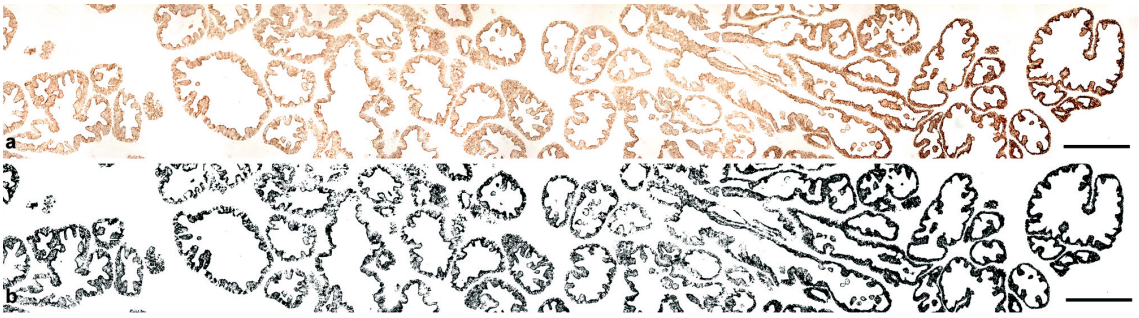

Fig. 1. In **(a)** the image shown is a strip from a specimen of CTR group immunostained to ck18. In **(b)** the binarized picture from **(a)** is depicted, the ck18 immunoreactive cytoplasm is in black and the space of reference (acinar lumina and stroma) in white. The scale bars: 110 μm.

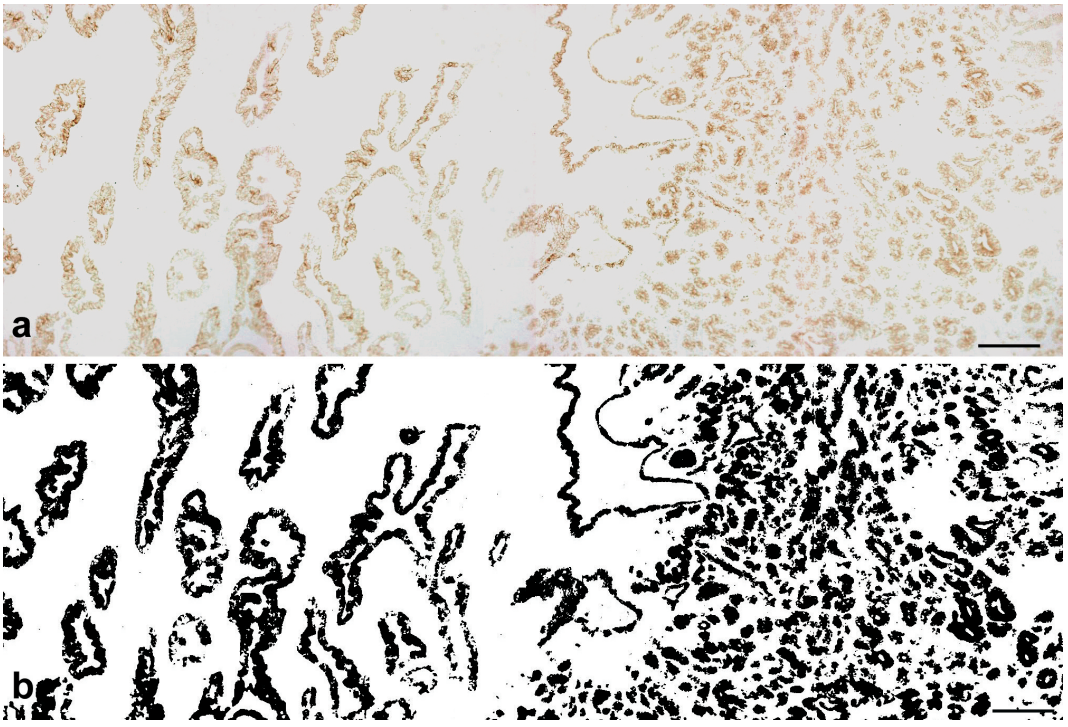

Fig. 2. In **(a)** the image shown is a strip from a specimen of Ca group immunostained to ck18. In **(b)** the binarized picture from **(a)** is depicted, the ck18 immunoreactive cytoplasm is in black and the space of reference (acinar lumina and stroma) in white. The scale bars: 110 μm.

Estimation of local variability of V_V ck18

The local variance for V_V ck18, related to the position, was measured in both CTR and Ca groups using wavelet analysis. The quadrat variance methods calculate the variance of differences among blocks of data of different sizes or scales and use the pattern of the variance estimates to determine the scale of the pattern (Leps, 1990). Wavelet analysis is similar to many of the quadrat variance methods, although, in some ways, it is much more flexible. Wavelets have been heavily studied in mathematics and engineering for signal analysis and data compression, but have had limited use in biology (Bradshaw and Spies, 1992, 1994; Dale and Mah, 1998; Nakken 1999).

A wavelet function is a scalable windowing function whose integral equals zero. One way to think of this is that the wavelet function describes a template that can be scaled to the desired size, and then slid onto the space series of V_V ck18 values along the long axis of the strip. When the template fits the observed data well, the value of the wavelet transform at that position is high; when it does not, the value is low. Then, the adjusting of wavelet function over the space series, obtain the overall variance at a given position and scale (Rosenberg et al., 2011). In the present study, wavelet analysis was performed from one to a maximum scale specified as a percentage of the input data size (50%). The wavelet kernel employed was the Haar wavelet function (Haar 1910). Wavelet analysis of variance was performed using the PASSaGE software. The results for both CTR and Ca groups were shown plotting the variance values in function of position expressed in microns.

Multiscale entropy analysis (MSE)

For each case from both CTR and Ca groups, the resulting series of N consecutive rational numbers per visual field resulting from the estimate of V_V ck18 measurements (per pixel of tissue) were employed as space series from which multiscale entropy was calculated:

Consecutive coarse-grained space series were

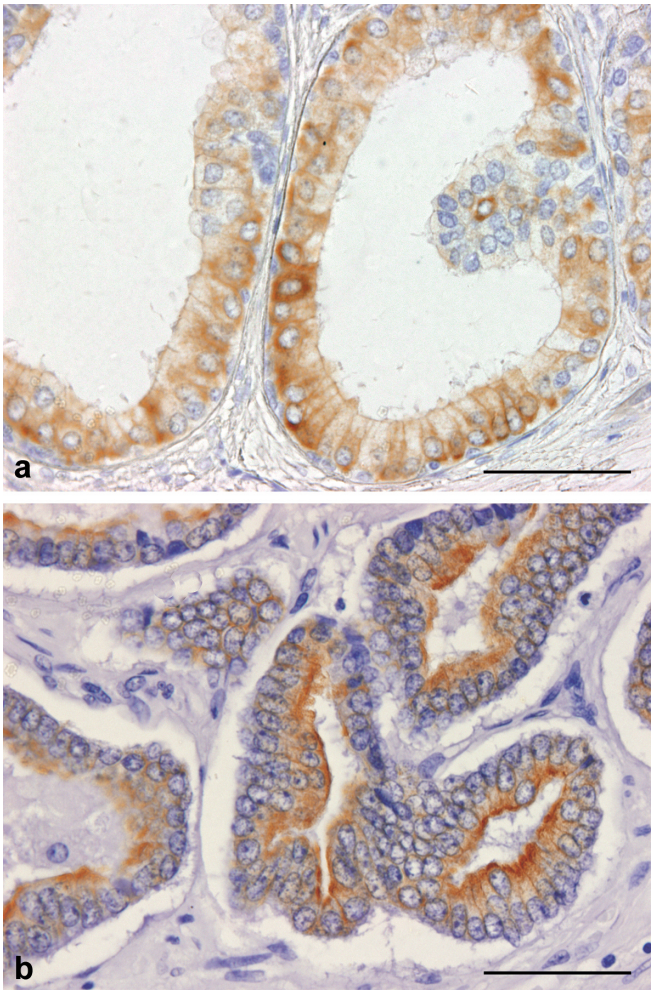

Fig. 3. Sections immunostained to ck18. In **(a)** image from a CTR case, in **(b)** an image from a cancer case where the immunostaining was mainly expressed at the apical border of the cells. The cell nuclei were counterstained with hematoxylin. The scale bars: 50 μm.

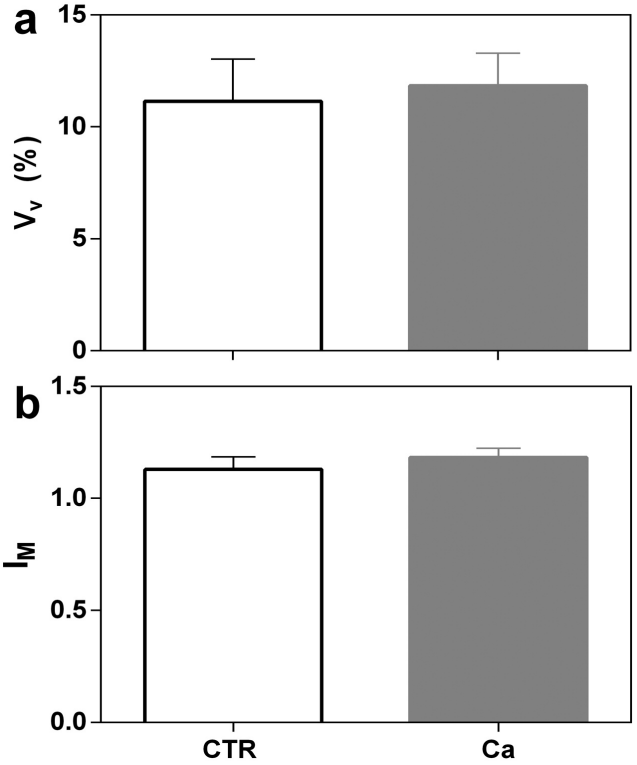

Fig. 4. Bar diagrams expressing mean ± SEM for **(a)** global V_V ck18. **b.** Morisita Index for dispersion of V_V ck18 global measures, in control (CTR) and cancer (Ca) groups.

constructed, given one-dimensional discrete space series, and using a scale factor, τ (ranged between 1 and 20). First, the original space series was divided into non-overlapping windows of length τ; second, the data points were averaged inside each window. For scale 1, the space series is merely the same as the original. The length of each coarse-grained space series is equal to the length of the original time series divided by the scale factor, τ. Finally, an entropy measure (sample entropy: S_E) was calculated for each coarse-grained space series plotted as a function of the scale factor τ. S_E is a "regularity statistic"; it looks for patterns in time or spatial series and quantifies its degree of predictability or regularity.

This procedure was called by their authors (Costa et al., 2000) multiscale entropy analysis (MSE). The MSE curves are used to compare the relative complexity of various space series. If for the majority of the scales the entropy values are higher for one space series than for another, the former is considered more complex than the latter, a monotonic decrease of the entropy values indicates the original signal contains information only at the smallest scale.

The values of the parameters used to calculate S_E are, m=2, and r=0.40. The parameter m represents the pattern length, this means that two data values of space series match each other, that is, they are indistinguishable if the absolute difference between them is ≤r. The value of the parameter r is a percentage of the space series SD, in the present study r represent the 15% of the average SD from CTR and Ca space series. This implementation corresponds to normalizing the space series. As a consequence, S_E results do not depend on the variance of the original space series, i.e., the absolute value of the data points, but only on their sequential ordering (Costa et al., 2005).

Randomization tests were performed to check whether the behavior of the observed data was random or followed a particular pattern (Santamaria et al., 2017). Randomization tests for MSE analysis work by randomizing the order of the quadrats within the space series and recalculating the MSE profile for the randomized data, this generates a null distribution of expected S_E values for data with the specific observed values but with no particular relationships. Significant S_E values can be identified from the observed data when the detected values fall outside the expectation generated from the randomization test.

All these calculations were implemented using the MSE software (Goldberger et al., 2000).

Statistical analysis

The global V_V ck18 and Morisita index were expressed as mean ± SEM. Comparisons between these means from CTR and Ca groups were performed by Student t-test. For V_V ck18 values along the space series, the positional variance of V_V ck18, and MSE analysis, the local estimates of mean ± SEM were performed and compared between CTR and Ca groups by Student t-test. The level of significance was $p<0.05$. For MSE analysis, the set of values showing significant differences between CTR and Ca was pooled and employed to perform stepwise linear discriminant analyses (Huisman et al., 2007) to determine whether locally estimated S_E was able to classify the cases accurately in CTR and Ca groups.

Discriminant variables were selected according to Wilk's lambda: at each step, the variable that minimizes the overall Wilk's lambda or maximizes the associated F statistic is selected (F to enter =3.84 and F to remove =2.71). Wilk's lambda statistic explains the rate of total variability that is not due to differences among groups. A lambda of 1 means that the mean of the discriminant scores is the same in all groups and there is no variability between groups, while a lambda near 0 implies that there is a significant difference among groups. Therefore, Wilk's lambda provides a test of the null hypothesis that the population means are equal. The

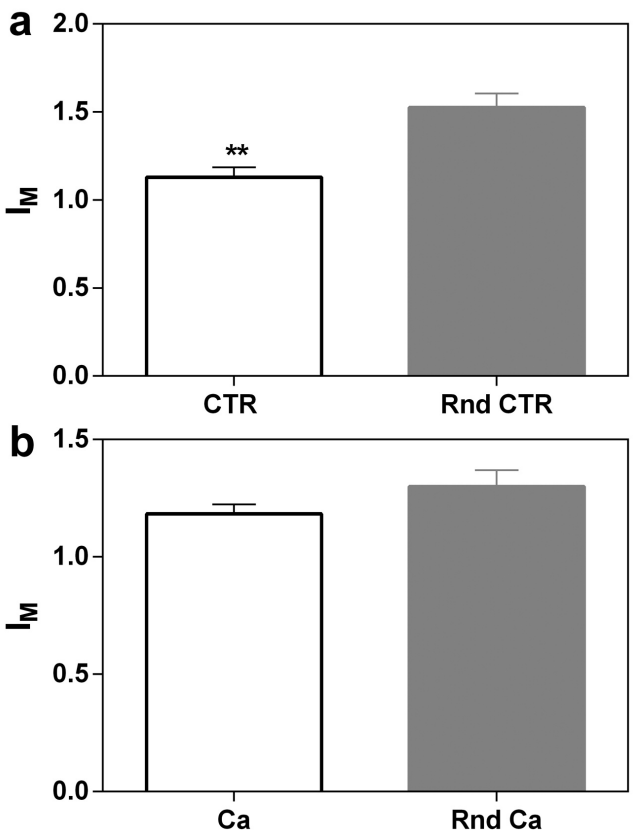

Fig. 5. Bar diagrams are expressing mean ± SEM for **(a)** Morisita Index for dispersion of V_V ck18 global measures, in control (CTR) group and a randomized series of controls (Rnd CTR). The asterisks over the error bar from CTR indicates that there are significant differences with Rnd CTR group (p=0.0012). **b.** Morisita Index for dispersion of V_V ck18 global measures, in cancer (Ca) group and a randomized series for cancer (Rnd Ca).

larger lambda is, the less discriminating power is present (Hair et al., 1998).

For each local variable, the discriminant scores obtained were used to construct relative frequency histograms for the CTR and Ca groups, to graphically show their ability to classify the cases.

Results

Immunohistochemistry

When comparing CTR with Ca cases, some differences were observed in ck18 immunoreactivity. In both groups, the immunostaining to ck18 was abundant and exclusively detected in columnar epithelial cells. Nevertheless, while in the CTR cases immunoexpression was detected diffusely throughout the cytoplasm, in Ca cases it was distributed mainly in the apical border of the cell (Fig. 3).

Global quantitative findings

No significant differences have been observed in global V_V ck18 and MI when CTR and Ca groups were compared (Fig. 4). MI estimated in CTR cases after randomization of the corresponding V_V ck18 space series was significantly higher than in the original cases (Fig. 5a). While for Ca group and randomized Ca group there were no significant differences (Fig. 5b).

Local quantitative findings

The estimate of local V_V ck18 (pixel by pixel) along the space series shows a similar profile in both CTR and Ca cases. Nevertheless, in several spaced segments of the strips from Ca group, V_V ck18 showed a significant increase in comparison with the same segment of the strip from CTR group (Fig. 6a). The segments of the Ca space series that show the above-indicated differences were in the next ranges of distance: 8916-8947; 9316-9515; 10061-10071; 10174-10386 microns (Fig. 6b).

The wavelet analysis indicated that positional variance of V_V ck18 was frequently higher in Ca than CTR (Fig. 7a), but these differences were significant only in several patches of the space series. The ranges (comprised between 6200 and 10000 microns) in which the positional variance was significantly different were: 6244-6812; 7822-8126; 8729-9121; 9203-9606; 9742-9907 microns (Fig. 7b).

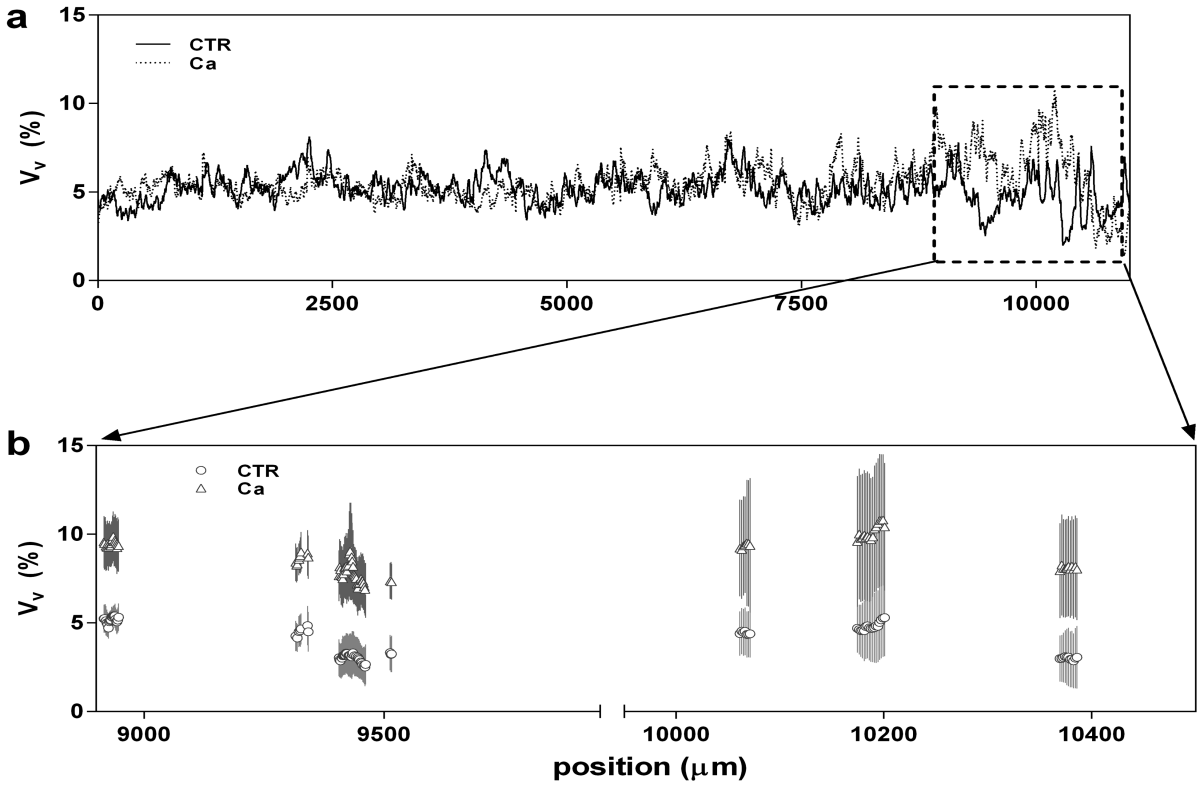

Fig. 6. a. Diagram for space series of local V_V ck18 values along the X-axis (position in μm) of the correspondent strips of CTR (continuous line) and Ca (dotted line) groups. The box with dotted borders contains the segment of space series were the differences between CTR and Ca are significant. **b.** More details of the inset (box) from **(a)**, the positions where the differences between CTR and Ca cases were significant are shown ($p<0.05$).

Multiscale entropy analysis

The estimate of MSE curves for V_V ck18 in both CTR and Ca groups shows in both groups an increase of S_E as a function of the scale factor, and differ significantly for MSE curves from a random distribution of the data (Fig. 8a,b). When comparing MSE between CTR and Ca cases, the Ca group shows higher significant values of S_E than CTR from scales larger than scale 2 (Fig. 8c).

The discriminant analyses applied to the MSE estimates for the groups of the study reveal that: From all the local S_E values showing significant differences (from scales 3 to 20) between CTR and Ca groups, only S_E at scales 3 and 5 have discriminatory power. With these two variables in the model, 91.3 % of the cases were correctly classified into the CTR and Ca groups. Table 1 shows the significant reduction of the Wilk's lambda statistic with these variables included in the model. The histograms show the distribution of the cases in CTR and Ca groups when the discriminant scores were applied (Fig. 9).

Discussion

The immunohistochemical findings observed in the present study are in part consistent with results by other authors (Nagle et al., 1987; Verhagen et al., 1992; Wolff et al., 1998), concerning the similarity of the

Table 1. Discriminant analysis to classify the CTR and Ca cases after local S_E.

Entered variable[1]	Wilks' lambda[2]	F[3]	p[4]
S_E (3)	0.433	27.453	<0.001
S_E (5)	0.332	20.092	<0.001

[1]Selected variables (S_E at scales 3 and 5 respectively). [2]This column shows the Wilks' lambda for every variable entered. [3]F distribution of Snedecor, the F minimum value for entering the variables was 3.84. [4]Level of significance p<0.05.

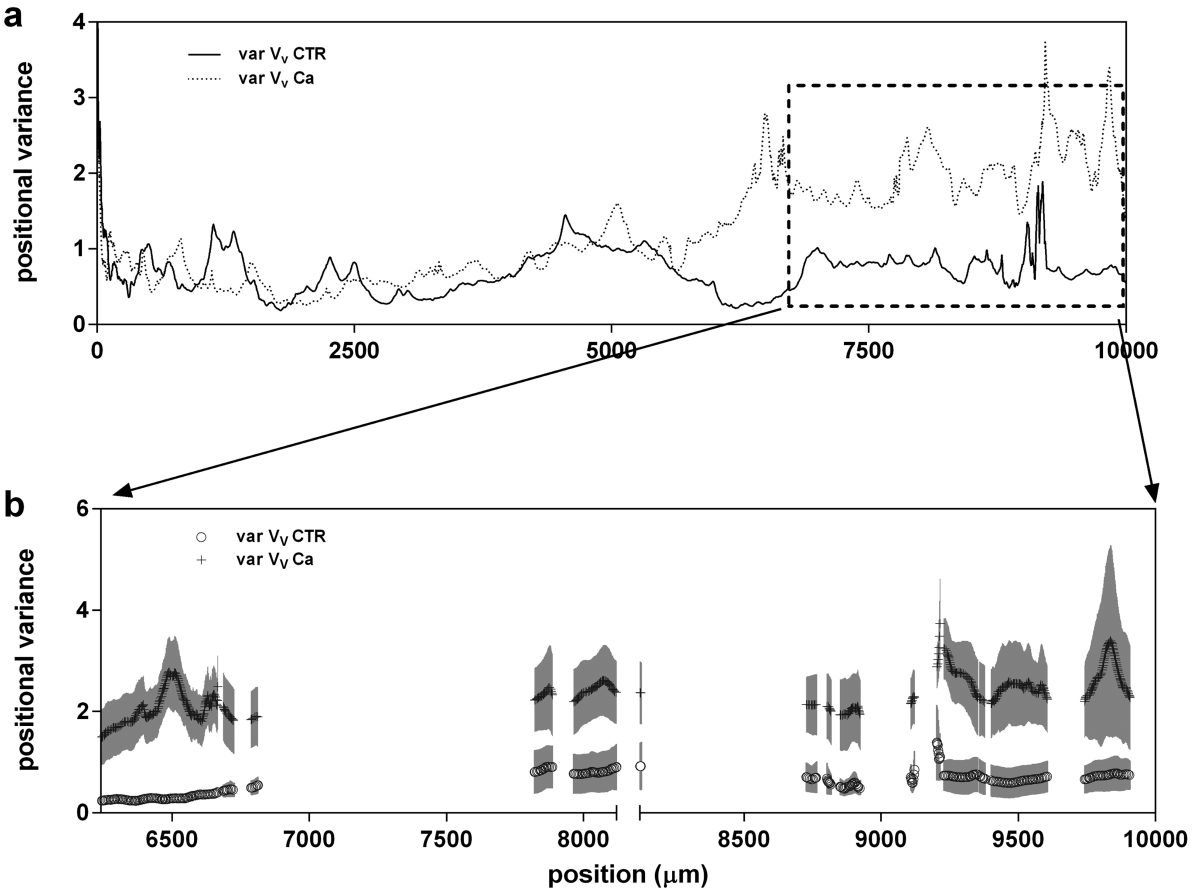

Fig. 7. a. Diagram for the positional variance from the space series of local V_V ck18 values along the X-axis (position in μm) of the correspondent strips of CTR (continuous line) and Ca (dotted line) groups. The box with dotted borders contains the segment of space series were the differences between CTR and Ca are significant. **b.** More details of the inset (box) from **(a)**, the positions where the differences of variance between CTR and Ca cases were significant are shown (p<0.05).

immunoexpression of ck18 in the luminal cells of the normal prostatic epithelium and the tumor cells in cancer. In this study, an apical predominance of immunoreactivity for ck18 in prostate cancer is frequently observed, which may be the consequence of a decrease in immunostaining in the rest of the cytoplasm. Other authors have described this decrease in the signal for ck18, in comparison with the expression of ck18 in non-tumor prostatic tissues (Festuccia et al., 2005).

The global quantification of the fraction of epithelial volume immunostained for ck18 (V_V ck18) in the Ca group does not show significant differences with the CTR group. This circumstance has also been described in benign prostatic hyperplasia (Santamaria et al., 2017). However, other authors (Panagiotaki et al., 2015) have observed that in the adenocarcinoma of the prostate an increase in the volume occupied by the tumor epithelium is detected in correlation with the decrease of the surrounding stroma. In any case, we can affirm that this increase of the epithelial compartment is not accompanied by an increase in the immunoexpression of ck18.

The Morisita Index did not show significant differences in the Ca group compared to the CTR group; this indicates that, unlike that observed for BPH (Santamaria et al., 2017), in prostate cancer, the acini immunoreactive for ck18 do not show a higher clumping than in the case of the normal prostate. An increase of the MI in the random distribution of the V_V ck18 is observed in comparison with the data of the original series. This increase is more evident for the CTR group and can be attributed to the tendency for spatial samples generated randomly to be clustered together, a statistical phenomenon well understood mathematically (Diggle 1983).

No global differences in V_V ck18 between CTR and Ca were observed. Nevertheless, at the local level, in limited segments of the space series of cases of the Ca group, a significant increase of V_V ck18 is detected compared to the normal prostate. The average length of the segments of the space series with significant differences for V_V ck18 represents less than 0.02% of the average of the total length. It is interesting to note that the increase in V_V ck18 in these regions was accompanied by a significant increase in its variability as detected by the wavelet analysis. This type of analysis has been scarcely used in prostate pathology (Jafari-Khouzani and Soltanian-Zadeh, 2003), but in our study, it has proved to be of interest for detection of local changes in the positional variance of V_V ck18. For all the space series, the positional variance was higher in Ca than CTR, but only in five segments (less of the 0.05% of the average of the total length) was this increase significant.

The increase in local variability of V_V ck18 can be related to the phenotypic variability of prostate cancer detected as spatial, genetic, and molecular heterogeneity (Humphrey 2004; Iczkowski et al., 2011; Tolkach and Kristiansen, 2018). Besides, local heterogeneity of the epithelial V_V ck18 can be put in parallel to those described for markers such as ki67, ck5, ck8, p65, and CD antigens (Liu et al., 2004; McDonnell et al., 2008; Mesko et al., 2013; Stoyanova et al., 2013).

It is interesting to note that the significant increase of both the local V_V ck18 and its variability in the Ca group always accumulated in an extreme position of the

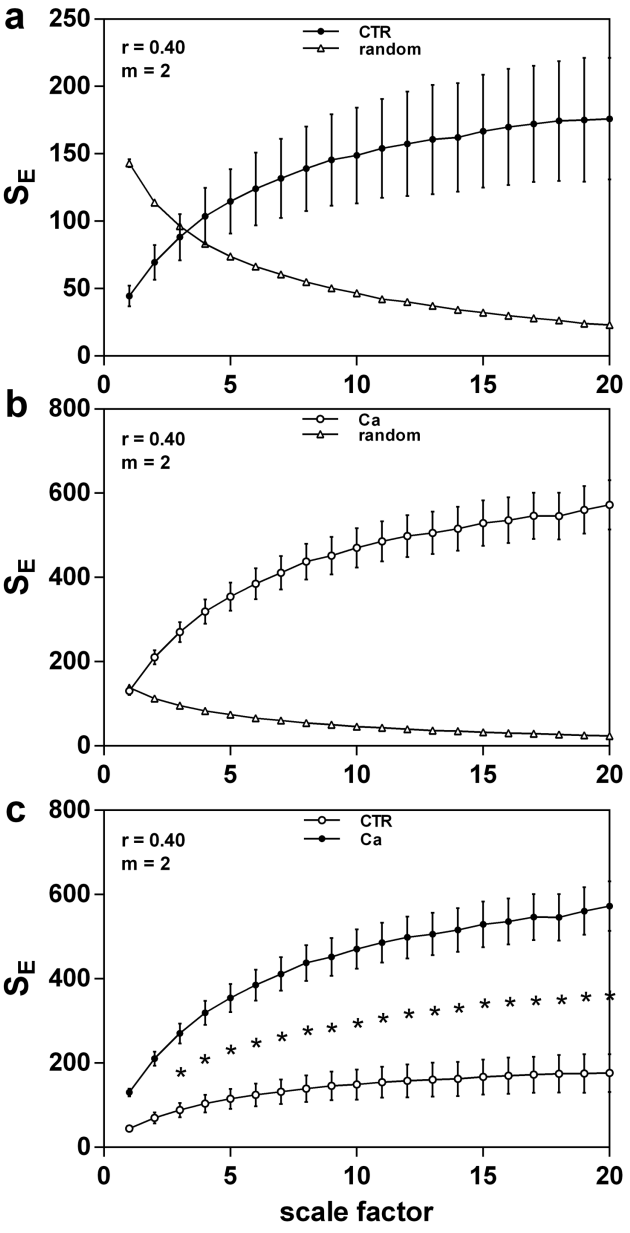

Fig. 8. MSE curves for V_V ck18 in CTR **(a)** and Ca groups **(b)** showing in both cases an increase of sample entropy (S_E) expressed as mean ± SEM, as a function of the scale factor. These MSE curves differ significantly from a random distribution of the data. In (c) the significant differences ($p<0.05$) for S_E between CTR and Ca are shown, from a scale factor =3.

space series, this could suggest that the distribution of the local values of V_V ck18 is asymmetric along the axis of the space series. This asymmetry may indicate the existence of anisotropy in the pattern of distribution of tumor acini.

In the MSE analysis, it is observed that in both CTR and Ca groups, the growth of S_E in function of the scale behaves according to a scaling law with a general form such as $Y \cong A \bullet X^B$. The entropy values are significantly higher in cancer than in the controls in an extensive range of spatial scales, and this suggests the presence of morphological processes in tumor cells that manifest a high degree of complexity. Of note, the weakest separation between the two groups occurs for scale one, the most robust separation is obtained for space scales higher than 10, as observed for other biological signals (Costa et al., 2002, 2005). The MSE algorithm was tested on a set of surrogate data obtained from the V_V ck18 space series from both CTR and Ca specimens by randomization of its data points. The MSE algorithm discriminated the two space series and revealed that the randomized surrogate data was less complex than the original data. These data agree with those observed by other authors (Teschendorff et al., 2015) that have indicated that if protein interaction networks were random graphs, described by Poisson degree distributions, that cancer would not exhibit an increased signaling entropy (Teschendorff et al., 2015). Furthermore, it assigned to the surrogate data set a behavior qualitatively similar to the one already described for white noise time series (Costa et al., 2002).

The increase in scale-dependent entropy detected for the local expression of ck18 in prostate cancer at the morphological level could be interpreted as the macroscopic expression of a similar growth at the molecular level (Teschendorff and Severini, 2010; Menichetti et al., 2015; Teschendorff et al., 2015). These studies have shown that signaling entropy, an overall measure of signaling pathway intertwining, correlates with phenotypic plasticity and is increased in cancer compared to normal tissue (Teschendorff et al., 2015).

It is well known that ck18 is not a biomarker for prostate carcinoma since it is a cytokeratin present in a multitude of epithelial cell lines, whether normal or pathological. What does seem interesting is that the phenotypic heterogeneity manifested by tumor cells also affects the expression of this class of cytokeratins.

The discriminant analysis has revealed that the increase of MSE in cancer only shows discriminatory power with the normal prostate at low scales (3 and 5) of the space series. That is, when the resolution decreases (coarse-grained series, i.e., higher scales), the S_E classificatory capacity also decreases. Therefore, not only the specific values of the entropy measure but also their dependence on resolution need to be taken into account to better characterize a pathologic process (Costa et al., 2002).

It is true that the accuracy of prostate cancer grading methods is very well established, particularly that of Gleason, although it usually does not reach 90% for biopsy samples when it correlates with the Gleason grading of the prostatectomy specimens. It appears that biopsy Gleason score, although often not corresponding strongly with the prostatectomy Gleason score, is an important prognostic factor in prostate cancer. There are significant differences in disease-free survival between biopsy and prostatectomy Gleason score categories (Narain et al., 2001; Stav et al., 2007). In any case, it is not the purpose of this study to present the MSE analysis as an additional method of diagnosis to standard procedures but rather highlight the regional heterogeneity of the local values of the volume fraction of tumor epithelium occupied by ck18.

The findings of the present study can be summarized, indicating that:

a.- The global quantification of the fraction of epithelial volume immunostained for ck18 in prostate cancer does not show significant differences in the

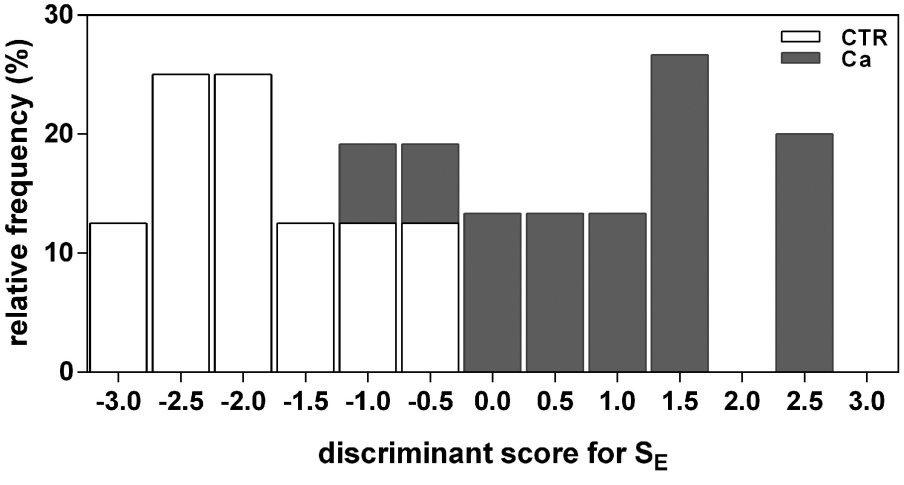

Fig. 9. Histogram showing the distribution of cases of CTR (void bars) and Ca (gray bars) groups when the discriminant scores obtained for S_E in the discriminant analysis were applied. 91% of cases were correctly classified in CTR and Ca groups.

normal prostate. However, changes in the expression of ck18 by the cancer prostate epithelium are not homogeneous.

b.- Unlike that observed for BPH, in prostate cancer, the acini immunoreactive for ck18 do not show a higher clumping than in the case of the normal prostate.

c.- The increase in local variability of ck18 immunoexpression can be related to the increase in heterogeneity of shape and size of the tumor acini observed in the advanced Gleason grading cancers.

d.- The distribution of the local values of V_V ck18 is asymmetric along the axis of the space series, this asymmetry may indicate the existence of anisotropy in the pattern of distribution of tumor acini.

e.- The increase in scale-dependent entropy detected for the local expression of ck18 in prostate tumor cells at the morphological level, could be interpreted as the macroscopic expression of the increase in entropy at the molecular level described in the tumor processes.

f.- The discriminant analysis shows that the dependence on the resolution for S_E values need to be taken into account to characterize the prostate cancer process better.

References

Armstrong R.A., Cairns N.J. and Lantos P.L. (2001). What does the study of the spatial patterns of pathological lesions tell us about the pathogenesis of neurodegenerative disorders?. Neuropathology 21, 1-12.

Baddeley A. and Vedel Jensen E. (2005). Uniform and isotropic uniform designs. In: Stereology for statisticians. Baddeley A. and Vedel Jensen E. (eds). Chapman & Hall, Boca Raton. pp 155-173.

Barwick K. and Mardi A. (1983). An immunohistochemical study of the myoepithelial cell in prostate hyperplasia and neoplasia. Lab. Invest. 48, 7A.

Bradshaw G.A. and McIntosh B.A. (1994). Detecting climate-induced patterns using wavelet analysis. Environ Pollut. 83, 135-142.

Bradshaw G.A. and Spies T.A. (1992). Characterizing canopy gap structure in forests using wavelet analysis. J. Ecol. 80, 205-215.

Brawer M.K., Peehl D.M., Stamey T.A. and Bostwick D.G. (1985). Keratin immunoreactivity in the benign and neoplastic human prostate. Cancer Res. 45, 3663-3667.

Costa M., Goldberger A.L. and Peng C.K. Multiscale Entropy Analysis (MSE). Electronic page: https://www.physionet.org. Last update: 2000. Availability: https://www.physionet.org/physiotools/mse/tutorial/tutorial.pdf. Date accessed: 15/4/18. 1-8.

Costa M., Goldberger A.L. and Peng C.K. (2002). Multiscale entropy analysis of complex physiologic time series. Phys. Rev. Lett. 89, 068102-1--068102-4.

Costa M., Goldberger A.L. and Peng C.K. (2003). Multiscale entropy analysis: a new measure of complexity loss in heart failure. J. Electrocardiol. 36, 39-40.

Costa M., Goldberger A.L. and Peng C.K. (2005). Multiscale entropy analysis of biological signals. Phys. Rev. E. Stat. Nonlin. Soft Matter Phys. 71, 021906-1--021906-17.

Dale M.R.T. and Mah M. (1998). The use of wavelets for spatial pattern analysis in ecology. J. Veg. Sci. 9, 805-881.

Diggle P.J. (1983). Statistical analysis of spatial point patterns. Mathematics in biology, Vol. 2. Academic Press. London. New York.

Epstein J.I., Allsbrook W.C. Jr, Amin M.B. and Egevad L.L. (2005). The 2005 International Society of Urological Pathology (ISUP) Consensus Conference on Gleason Grading of Prostatic Carcinoma. Am. J. Surg. Pathol. 29, 1228-1242.

Festuccia C., Angelucci A., Gravina G.L., Muzi P., Miano R., Vicentini C. and Bologna M. (2005). Epithelial and prostatic marker expression in short-term primary cultures of human prostate tissue samples. Int. J. Oncol. 26, 1353-1362.

Franke W.W., Appelhans B., Schmid E., Freudenstein C., Osborn M. and Weber K. (1979). Identification and characterization of epithelial cells in mammalian tissues by immunofluorescence microscopy using antibodies to prekeratin. Differentiation 15, 7-25.

Gao J., Hu J., Liu F. and Cao Y. (2015). Multiscale entropy analysis of biological signals: a fundamental bi-scaling law. Front. Comput. Neurosci. 9, 64.

Goldberger A.L., Amaral L.A.N., Glass L., Hausdorff J.M., Ivanov P.Ch., Mark R.G., Mietus J.E., Moody G.B., Peng C.K. and Stanley H.E. (2000). PhysioBank, PhysioToolkit, and PhysioNet: components of a new research resource for complex physiologic signals. Circulation 101, e125-e220.

Gundersen H.J. and Osterby R. (1981). Optimizing sampling efficiency of stereological studies in biology: or 'do more less well'. J. Microsc. 121, 65-73.

Haar A. (1910). Zur theorie der orthogonalen funktionen-systeme. Mathematische Annalen 69, 331-371.

Hair J.F., Anderson R.E., Tatham R.L. and Black W.C. (1998). Multivariate data analysis, 5 ed. Prentice Hall, Upper Saddle River, New Jersey (USA).

Howard C.V. and Reed M.G. (2005). Unbiased Stereology: three-dimensional measurement in microscopy, 2 ed. Bios Scientific Publishers. Oxford.

Huisman A., Ploeger L.S., Dullens H.F., Jonges T.N., Belien J.A., Meijer G.A., Poulin N., Grizzle W.E. and van Diest P.J. (2007). Discrimination between benign and malignant prostate tissue using chromatin texture analysis in 3-D by confocal laser scanning microscopy. Prostate 67, 248-254.

Humphrey P.A. (2004). Gleason grading and prognostic factors in carcinoma of the prostate. Mod. Pathol. 17, 292-306.

Iczkowski K.A., Torkko K.C., Kotnis G.R., Wilson R.S., Huang W., Wheeler T.M., Abeyta A.M. and Lucia M.S. (2011). Pseudolumen size and perimeter in prostate cancer: correlation with patient outcome. Prostate Cancer 2011, 1-5.

Jafari-Khouzani K. and Soltanian-Zadeh H. (2003). Multiwavelet grading of pathological images of prostate. IEEE Trans. Biomed Eng. 50, 697-704.

Leps J. (1990). Comparison of transect methods for the analysis of spatial pattern. In: Spatial processes in plant communities. Kraulec F., Agnew A.D.Q., Agnew S. and Willem J.H. (eds). Academia Press. Prague. pp 71-82.

Liu A.Y., Roudier M.P. and True L.D. (2004). Heterogeneity in primary and metastatic prostate cancer as defined by cell surface CD profile. Am. J. Pathol. 165, 1543-1556.

Martin J.J., Martin R., Codesal J., Fraile B., Paniagua R. and Santamaria L. (2001). Cadmium chloride-induced dysplastic changes in the ventral rat prostate: an immunohistochemical and quantitative study. Prostate 46, 11-20.

McDonnell T.J., Chari N.S., Cho-Vega J.H., Troncoso P., Wang X., Bueso-Ramos C.E., Coombes K., Brisbay S., Lopez R., Prendergast

G., Logothetis C. and Do K.A. (2008). Biomarker expression patterns that correlate with high grade features in treatment naive, organ-confined prostate cancer. BMC Med. Genomics 1, 1-9.

Menichetti G., Bianconi G., Castellani G., Giampieri E. and Remondini D. (2015). Multiscale characterization of ageing and cancer progression by a novel network entropy measure. Mol. Biosyst. 11, 1824-1831.

Mesko S., Kupelian P., Demanes D.J., Huang J., Wang P.C. and Kamrava M. (2013). Quantifying the ki-67 heterogeneity profile in prostate cancer. Prostate Cancer 717080, 1-5.

Moll R., Franke W.W., Schiller D.L., Geiger B. and Krepler R. (1982). The catalog of human cytokeratins: patterns of expression in normal epithelia, tumors and cultured cells. Cell 31, 11-24.

Morisita M. (1959). Measuring the dispersion and the analysis of distribution patterns. Memoires of the Faculty of Science. Kyushu University, Series E Biology 2, 215-235.

Nagle R.B., Ahmann F.R., McDaniel K.M., Paquin M.L., Clark V.A. and Celniker A. (1987). Cytokeratin characterization of human prostatic carcinoma and its derived cell lines. Cancer Res. 47, 281-286.

Nakken M. (1999). Wavelet analysis of rainfall-runoff variability isolating climatic from anthropogenic patterns. Environ. Model Software 14, 283-295.

Narain V., Bianco F.J. Jr, Grignon D.J., Sakr W.A., Pontes J.E. and Wood D.P. Jr (2001). How accurately does prostate biopsy Gleason score predict pathologic findings and disease free survival? Prostate 49, 185-190.

Panagiotaki E., Chan R.W., Dikaios N., Ahmed H.U., O'Callaghan J., Freeman A., Atkinson D., Punwani S., Hawkes D.J. and Alexander D.C. (2015). Microstructural characterization of normal and malignant human prostate tissue with vascular, extracellular, and restricted diffusion for cytometry in tumours magnetic resonance imaging. Invest. Radiol. 50, 218-227.

Park Y., Lim S., Nam J.W. and Kim S. (2016). Measuring intratumor heterogeneity by network entropy using RNA-seq data. Sci. Rep. 6, 37767.

Quinlan R.A., Schiller D.L., Hatzfeld M., Achtstatter T., Moll R., Jorcano J.L., Magin T.M. and Franke W.W. (1985). Patterns of expression and organization of cytokeratin intermediate filaments. Ann. NY Acad. Sci. 455, 282-306.

Rasband W.S. and Bright D.S. (1995). NIH image: A public domain image processing program for the Macintosh. Microbeam. Anal Soc. J. 4, 137-149.

Rosenberg M.S. and Anderson C.D. (2011). Application PASSaGE: Pattern Analysis, Spatial Statistics and Geographic Exegesis. Version 2. Methods Ecol. Evol. 2, 229-232.

Santamaria L., Ingelmo I., Ruiz J. and Teba F. (2011). Study of the distribution of microvessels in normal and pathologic prostate using an information-based similarity analysis. J. Microsc. 243, 303-314.

Santamaría L., Ingelmo I., Teba F., Rodríguez R. and Pozuelo JM. (2015). Estimate of the pair correlation functions of nuclei in normal prostate, prostatic intraepithelial neoplasia, and cancer. Eur. J. Anat. 19, 361-370.

Santamaria L., Ingelmo I., Teba F., Coloma A. and Martínez L. (2016). Quantitative stereological estimations of structural patterns of the glandular tree in benign hyperplasia of prostate. Open J. Pathol. 6, 122-133.

Santamaria L., Ingelmo I. and Teba F. (2017). Structural patterns of immunoreactivity to cytokeratin 18 in normal prostate and benign prostate hyperplasia: Global and local differences. Open J. Pathol. 7, 25-44.

Santamaría Solis L., Ingelmo Ingelmo I., Rodríguez Ramos L., Sinues Ojas B., Martínez Blázquez L. and Teba del Pino F. (2015). Estimate of the K function and isotropy of acini in human normal prostate and prostate adenocarcinoma. Histol. Histopathol. 30, 149-150.

Schlegel R., Banks-Schlegel S. and Pinkus G.S. (1980). Immunohistochemical localization of keratin in normal human tissues. Lab. Invest. 42, 91-96.

Stav K., Judith S., Merald H., Leibovici D., Lindner A. and Zisman A. (2007). Does prostate biopsy Gleason score accurately express the biologic features of prostate cancer?. Urol. Oncol. 25, 383-386.

Stoyanova T., Cooper A.R., Drake J.M., Liu X., Armstrong A.J., Pienta K.J., Zhang H., Kohn D.B., Huang J., Witte O.N. and Goldstein A.S. (2013). Prostate cancer originating in basal cells progresses to adenocarcinoma propagated by luminal-like cells. Proc. Natl. Acad. Sci. USA 110, 20111-20116.

Teschendorff A.E. and Severini S. (2010). Increased entropy of signal transduction in the cancer metastasis phenotype. BMC Syst. Biol. 4, 104.

Teschendorff A.E., Banerji C.R., Severini S., Kuehn R. and Sollich P. (2015). Increased signaling entropy in cancer requires the scale-free property of protein interaction networks. Sci. Rep. 5, 9646.

Tolkach Y. and Kristiansen G. (2018). The heterogeneity of prostate cancer: A practical approach. Pathobiology 31, 1-9.

Verhagen A.P., Ramaekers F.C., Aalders T.W., Schaafsma H.E., Debruyne F.M. and Schalken J.A. (1992). Colocalization of basal and luminal cell-type cytokeratins in human prostate cancer. Cancer Res. 52, 6182-6187.

Wolff J.M., Borchers H., Brehmer B. Jr, Brauers A. and Jakse G. (1998). Cytokeratin 8/18 levels in patients with prostate cancer and benign prostatic hyperplasia. Urol. Int. 60, 152-155.

Accepted June 4, 2018